Accepted for publication in ApJ
Preprint typeset using LaTeX style emulateapj v. 5/2/11

ALMA OBSERVATIONS OF A MISALIGNED BINARY PROTOPLANETARY DISK SYSTEM IN ORION

Jonathan P. Williams[1], Rita K. Mann[2], James Di Francesco[2,3], Sean M. Andrews[4], A. Meredith Hughes[5], Luca Ricci[4], John Bally[6], Doug Johnstone[2,3,7], and Brenda Matthews[2,3]

Accepted for publication in ApJ

ABSTRACT

We present *ALMA* observations of a wide binary system in Orion, with projected separation 440 AU, in which we detect submillimeter emission from the protoplanetary disks around each star. Both disks appear moderately massive and have strong line emission in CO 3–2, HCO^+ 4–3, and HCN 3–2. In addition, CS 7–6 is detected in one disk. The line-to-continuum ratios are similar for the two disks in each of the lines. From the resolved velocity gradients across each disk, we constrain the masses of the central stars, and show consistency with optical-infrared spectroscopy, both indicative of a high mass ratio ~ 9. The small difference between the systemic velocities indicates that the binary orbital plane is close to face-on. The angle between the projected disk rotation axes is very high, $\sim 72°$, showing that the system did not form from a single massive disk or a rigidly rotating cloud core. This finding, which adds to related evidence from disk geometries in other systems, protostellar outflows, stellar rotation, and similar recent *ALMA* results, demonstrates that turbulence or dynamical interactions act on small scales well below that of molecular cores during the early stages of star formation.

Subject headings: circumstellar matter — protoplanetary disks — stars: pre-main sequence

1. INTRODUCTION

About one in two stars of solar mass and greater are born in pairs (Duchêne & Kraus 2013). Because of their common origin and age, young stellar binaries provide useful benchmarks for understanding star formation and evolution, and are extensively studied (Mathieu 1994). Circumstellar disks can exist around the individual stars in wide systems with semi-major axes $\gtrsim 100$ AU, with masses and lifetimes that are similar to those around single stars (Jensen et al. 1996; Cieza et al. 2009; Kraus et al. 2012; Harris et al. 2012) and apparently similar planetary end-products (Desidera & Barbieri 2007).

Circumstantial evidence has long suggested that the rotation axes of such wide binaries are mis-aligned. These include measurements of stellar rotation (Hale 1994) and non-parallel protostellar jets (e.g., Lee et al. 2002; Chen et al. 2008). More recently, detailed modeling of infrared interferometry and spectral energy distributions have indicated non-aligned disk planes in the T Tau (Ratzka et al. 2009), and GV Tau (Roccatagliata et al. 2011) systems. With the advent of the Atacama Large Millimeter/Submillimeter Array (*ALMA*), the rotation of individual disks in wide binary systems has now been directly measured and shown to be misaligned in HK Tau (Jensen & Akeson 2014) and AS 205 (Salyk et al. 2014). These observations demonstrate that wide binaries do not form in large, co-rotating structures and indicate the importance of stochastic processes during the early phases of star formation, either gas turbulence or dynamical interactions of young protostars. Planetary systems that form in such mis-aligned systems may be subject to secular torques that can affect their orbital evolution (Batygin 2012).

The subject of this paper is V2434 Ori in the M43 HII region of Orion. *HST* imaging by Smith et al. (2005) reveal this to be a binary system with an angular separation of 1.″1, corresponding to 440 AU at our assumed distance to Orion of 400 pc (Sandstrom et al. 2007; Menten et al. 2007). The optically fainter component is surrounded by a large silhouette disk and drives a jet with associated Herbig-Haro (HH 668) objects. Following the naming convention for *HST*-identified protoplanetary disks ("proplyds") proposed by O'dell & Wen (1994), we refer to the system as 253-1536.

The discovery that both binary members have disks was made by Mann & Williams (2009) though submillimeter imaging. The two disks were subsequently detected at 7 mm by Ricci et al. (2011) and the near-blackbody millimeter colors indicate that both harbor a substantial population of large dust grains, characteristic of protoplanetary disks. Following the nomenclature in those papers, we denote the brighter millimeter source as component A, although it is the fainter optical source. Here we present new *ALMA* observations that reveal the molecular line emission from the disks. These data allow us to examine disk masses, kinematics, and chemistry, as well as constrain the masses of their central stars. Similar to the aforementioned HK Tau and AS 205 results, we find here that the disks in this system are strongly misaligned. The observations are described in §2, the results are presented in §3, and the implications are discussed in §4.

[1] Institute for Astronomy, University of Hawaii, Honolulu, HI 96816, USA; jpw@ifa.hawaii.edu
[2] NRC Herzberg Astronomy and Astrophysics, 5071 West Saanich Road, Victoria, BC, V9E 2E7, Canada
[3] Department of Physics and Astronomy, University of Victoria, Victoria, BC, V8P 1A1, Canada
[4] Harvard-Smithsonian Center for Astrophysics, 60 Garden Street, Cambridge, MA 02138, USA
[5] Van Vleck Observatory, Astronomy Department, Wesleyan University, 96 Foss Hill Drive, Middletown, CT 06459, USA
[6] CASA, University of Colorado, CB 389, Boulder, CO 80309, USA
[7] Joint Astronomy Centre, 660 North Aohoku Place, University Park, Hilo, HI 96720, USA

2. OBSERVATIONS

The data analyzed here come from the fifth field observed in the *ALMA* Cycle 0 (project 2011.0.00028.S) study of the Orion proplyds by Mann et al. (2014) wherein the details of the data acquisition and reduction can be found. That paper discusses the disk dust masses as inferred from the 856 μm (350.5 GHz) continuum but here we focus on the molecular lines observed in same observations; CO 3–2 and CS 7–6 in the lower sideband, and HCO^+ 4–3, and HCN 4–3 in the upper sideband. The Hanning smoothed spectral resolution of these data is $d\nu = 488.28$ kHz corresponding to velocity channels of $dv \simeq 0.42$ km s^{-1}.

The full extent of the two disks in the binary system is less than the maximum recoverable scale of 5″ so no emission is resolved out. The resolution of the continuum and line maps, $\sim 0\farcs5$, is lower than the Submillimeter Array (*SMA*) images of Mann & Williams (2009) but the sensitivity of the *ALMA* data is much higher, allowing us to detect all four molecular lines and to measure velocity gradients within each disk.

3. RESULTS

3.1. *Moment Maps*

Maps of the submillimeter continuum, optical *HST* image, and molecular lines are displayed in Figure 1. Both disks are clearly detected in the continuum, CO 3–2, HCO^+ 4–3, and HCN 4–3. The large silhouette disk around 253-1536A, the brighter millimeter source, is also detected in CS 7–6. The positions of the two continuum peaks are given in Table 1.

The mapped area (primary beam) is much larger than the region shown in Figure 1. From inspection of the full maps, we see strong CO emission over a range of size scales from the background molecular cloud but much weaker emission in the other lines. The CO contamination affects the disk morphologies, which show a small offset between line and continuum peaks, and the resulting flux measurements. However, the contamination in the other lines is negligible. The uncontaminated HCO^+ line is in fact the strongest line in the bandpass. The HCN line is $\sim 4-5$ times weaker, and the CS line > 25 times weaker.

The continuum and integrated line fluxes for each disk are given in Table 2. The error due to flux calibration is estimated to be about 10% (Mann et al. 2014). The continuum flux density is stronger than that measured by the *SMA* measurements by Mann & Williams (2009), partly due to the slightly shorter observing wavelength but mostly to the greater quality (phase coherence and signal-to-noise ratio) of the *ALMA* data. The CO fluxes are unreliable measures of the true disk emission due to the aforementioned cloud confusion. The main uncertainty in the fluxes of the other lines, estimated to be about 20%, is in separating the overlap between the two disks as the detectable gas emission extends further than the dust (e.g., Hughes et al. 2008; Andrews et al. 2012).

The first moment (intensity weighted mean velocity) of each line is shown in the right panels of Figure 1 and reveal consistent velocity gradients across both disks. The direction of the gradients in the two disks are very different from each other, which indicates that they do not share the same axis of rotation. We use the HCO^+ data to analyze the velocity structure in more detail as they provide the best combination of high signal-to-noise ratio and low cloud confusion.

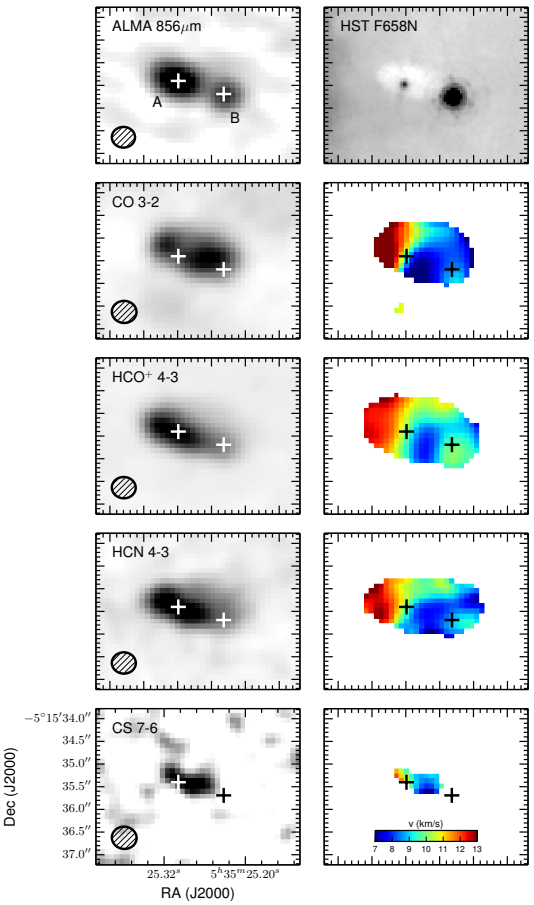

Figure 1. Images of the continuum and line data. The top row shows the *ALMA* continuum emission at the central observing wavelength of 856 μm, and the *HST* image in the F658 narrow band (Hα) filter. The *HST* image shows the two stars and the large silhouette disk around the fainter source, labeled component A on account of its brighter millimeter emission. A faint optical jet is seen perpendicular to the disk, and a diffraction pattern is seen around the optically brighter component B. The *ALMA* image shows disk dust emission from both binary members. The lower four rows show velocity moment 0 and 1 maps for the four observed lines. Line emission from CO 3–2, HCO^+ 4–3, and HCN 4–3 is detected toward both disks, and CS 7–6 toward the large silhouette disk around component A. The velocity maps are on the same scale, 7 to 13 km s^{-1}, and show a similar pattern of gradients across each source but oriented in very different directions.

Table 1
Continuum source positions

Source	R.A.	Dec.
253-1536A	05:35:25.30	-05:15:35.40
253-1536B	05:35:25.23	-05:15:35.69

3.2. *Analysis of HCO^+ data*

Channel maps of the HCO^+ 4–3 emission are plotted in Figure 2. These more clearly show the velocity gradients across each of the two sources and the difference in the

Table 2
Integrated Flux Measurements

Line	253-1536A	253-1536B	Units
Continuum[a]	0.163	0.061	Jy
CO 3–2[b]	5.9	2.1	Jy km s^{-1}
HCO$^+$ 4–3[c]	10.5	2.7	Jy km s^{-1}
HCN 4–3[c]	2.6	0.6	Jy km s^{-1}
CS 7–6[c]	0.2	< 0.1	Jy km s^{-1}

[a] Uncertainty due to flux calibration $\sim 10\%$.
[b] Unreliable measures of disk emission due to strong cloud contamination.
[c] Uncertainty $\sim$ 30% due to flux calibration and source overlap.

angle between them.

To measure the size and direction of the velocity gradient, we fit elliptical gaussians to the channel maps as in Tobin et al. (2012). The centroids of the fits toward the two sources are shown, color-coded by velocity, in Figure 3. The reversal of the centroids at the lowest and highest velocities toward the large silhouette disk around 253-1536A is a clear signature of gravitational motion; the gas moves faster closer to the star. Because of the weaker emission toward 253-1536B, fewer channels were detected and we are unable to see the same signature. Given the strength and small velocity extent of the HCO$^+$ and HCN lines, however, we assume that they similarly trace the kinematics of the dusty disk rather than an outflow.

Through linear fits to the positions of the centroids, we determine the projected rotational planes of the two disks. Following the convention that the position angle (PA) is measured east of north to the redshifted edge of the disk we find $PA_{\rm A} = 69.7 \pm 1.4°$ and $PA_{\rm B} = 136 \pm 15°$ for components A and B respectively[8]. These are projections and the true angle between the rotational axes of the disks (derived from the dot product of the angular momentum vectors) depends on the inclinations

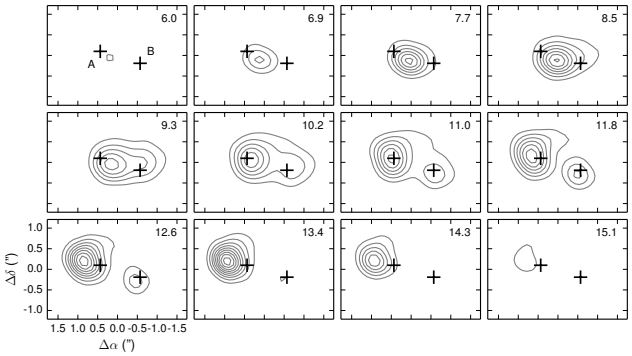

Figure 2. Contours of HCO$^+$ 4–3 emission in velocity channels from 6 to 15 km s^{-1}. The contour levels start at and increase by 0.1 Jy km s^{-1}. The source central positions are indicated by crosses and labeled in the upper left panel. The velocity of each channel (in km s^{-1}) is given in the upper right corner of each panel.

[8] As the data are Hanning smoothed, we binned the velocity channels by 2 to provide independent points for the purpose of making the linear fits.

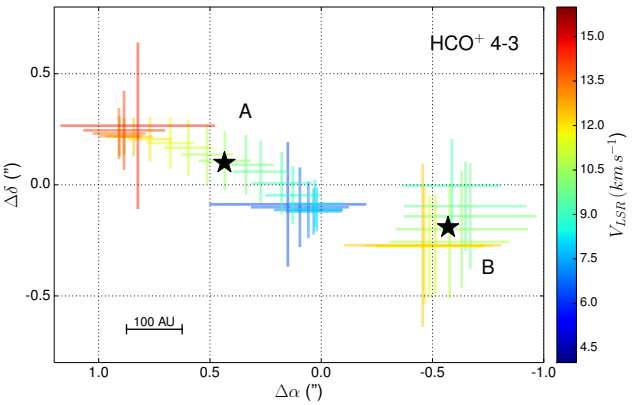

Figure 3. The centroids of each velocity channel in the HCO$^+$ 4–3 datacube. The cross displays the center and uncertainty associated with an elliptical gaussian fit to each channel, and the color indicates the velocity as shown by the scale on the right hand side. There are clear gradients in the disks around both sources, and the projected rotational angles are almost perpendicular to each other. The highest velocity channels for component A are closer to the star than slightly lower velocities indicative of gravitational motion.

of the two disks,

$$\cos\Delta = \cos i_{\rm A}\ \cos i_{\rm B} + \sin i_{\rm A}\ \sin i_{\rm B}\ \cos(PA_{\rm A} - PA_{\rm B}), \quad (1)$$

as in Jensen & Akeson (2014). For the resolved silhouette disk, 253-1536A, we determine an inclination from face-on, $i_{\rm A} = 65 \pm 5°$, based on the $0\farcs6 \times 1\farcs4$ size of the optical shadow (Smith et al. 2005), but the inclination of the unresolved disk, 253-1536B, is unknown and can vary from 0° to 180° where 90° is edge-on. We plot the angle, Δ, as a function of this inclination in the left panel of Figure 4. For random orientations, the probability of a particular inclination is proportional to the sine of the inclination (i.e., edge-on disks are more common than face-on). Using this as a prior, and without attempting to fit the observations further, we plot the posterior probability distribution for Δ in the right panel of Figure 4 and derive a mean value and standard deviation, $\Delta = 72° \pm 20°$. Thus we can robustly conclude that the disks are indeed strongly mis-aligned.

The projected radius from the star is plotted against the channel velocity for the silhouette disk around 253-1536A in Figure 5. The S-shape is due to a combination of resolution, sensitivity, and Keplerian rotation. Because the disk is inclined and not resolved along the minor axis, emission at velocities close to the systemic motion of the star is dominated by the bright emission from the inner regions of the disk that project to low radial velocities (rather than the fainter emission from the slower moving outer disk) and channel maps only show slight offsets with respect to the star. There is less confusion at greater relative velocities but also weaker emission. There are a few low and high velocity channels, however, for which we can detect the increasing rotational velocity closer to the star. These are marked in blue and compared with a Keplerian profile,

$$v_{\rm LSR} = v_{\rm sys} + \left(\frac{GM_*}{R}\right)^{1/2} \sin i, \quad (2)$$

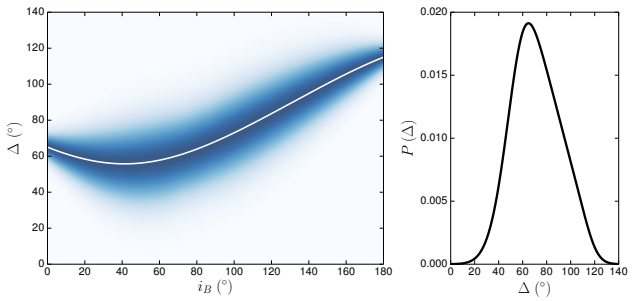

Figure 4. The left panel shows the angle, Δ, between the disk rotational axes, as a function of the unknown inclination of the unresolved source 253-1536B, i_B. The (assumed gaussian) uncertainty at each value is illustrated by blue shading, and is due to the errors in the measured inclination of source A and projected position angles of the two disks. The right panel shows the posterior probability (per degree) of Δ given a prior for the inclination, $P(i_B) \propto \sin(i_B)$.

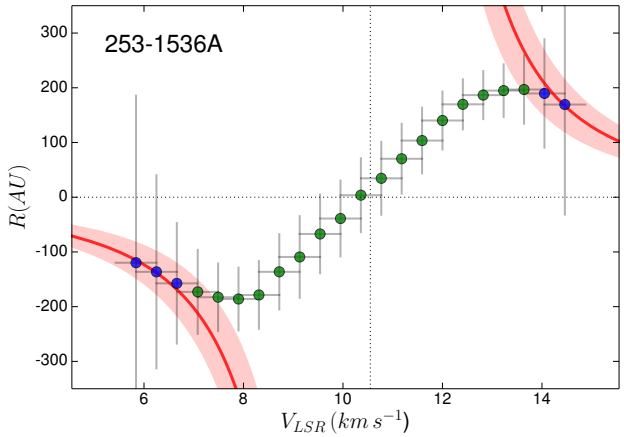

Figure 5. The distance from the star in binary component A for each velocity channel of the disk HCO^+ emission. The reversal in distance at the greatest speeds away from systemic are shown as blue points and compared with Keplerian profiles for a star with mass $M_{star} = 3.5\,M_\odot$ (solid red line) and range $\pm 1\,M_\odot$ (light red shaded region).

in Figure 5 to provide a rough estimate of the central stellar mass. The resolution and signal-to-noise ratio of the data are insufficient to attempt a more detailed model and more rigorous fitting as in e.g., Rosenfeld et al. (2012). With a well constrained inclination, $i_A = 65°$, as discussed above, we infer $M_* \sim 3.5\,M_\odot$.

The moderately high stellar mass for this optically faint star is consistent with the X-Shooter ultraviolet-optical-infrared spectrum discussed by Ricci et al. (2011). The lack of prominent absorption lines led them to conclude that the star is heavily veiled and is spectral type F or G. For an age range of 1–3 Myr, this corresponds to a mass, $M_* \sim 2.5 - 4\,M_\odot$.

We can similarly look at the rotation curve for 253-1536B. The disk emission is weaker, both in the line and continuum, and we do not resolve it spatially. However, we are able to measure a shift in the peak position in different spectral channels and from this can study its kinematics. Although we do not detect a Keplerian turnover, the velocity gradient in Figure 3 provides a lower limit to the stellar mass, $M_* \gtrsim 0.2\,M_\odot / \sin^2 i_B$. This is consistent with the spectral typing of an M2 star ($M_* \sim 0.4\,M_\odot$ for an age range 1-3 Myr) from the X-Shooter spectrum (Ricci et al. 2011) and the catalog of Hillenbrand (1997), which classifies it as M2.5e (source 767). Both sets of authors note emission lines in the spectrum that are signatures of strong accretion.

The central velocities of 253-1536A and B are v_{sys} = 10.55 and 10.85 km s^{-1} respectively, with errors of about 0.1 km s^{-1}. The escape speed of the two stars from one another is $\sim$ 2.5 km s^{-1} at the projected separation of 440 AU, and greater than the measured 0.3 km s^{-1} difference unless the system is $\gtrsim 10^4$ AU apart and viewed almost edge-on. However, the probability of a chance alignment of the two stars was already known to be low (see discussion in Mann & Williams 2009) and this additional kinematic information more likely indicates that this is a bound binary system with an orbital plane close to face-on.

4. SUMMARY AND DISCUSSION

The tremendous increase in sensitivity that *ALMA* provides is transforming our view of protoplanetary disks. Whereas we had known of the existence of the two disks under study here from *SMA* continuum observations, we can now detect their line emission and study their kinematics. The magnitude of the measured velocity gradients provides bounds on the central masses that are consistent with stellar spectroscopy. The system has a very high mass ratio, ~ 9, that makes it a useful laboratory for studying the dependence of disk properties on stellar mass.

From the continuum alone, we estimate disk masses of 0.074 $M_\odot$ and 0.028 $M_\odot$ for sources 253-1536A and B respectively, assuming canonical values for the temperature, dust opacity and an ISM gas-to-dust ratio of 100 (Williams & Cieza 2011). Under these assumptions, the disk to stellar mass ratios are $\sim$ 2% and $\sim$ 7% respectively. This is particularly high for for the M2 star, 253-1536B, but the dust is likely warmer than the canonical 20 K (possibly in both disks) given the high stellar mass and therefore luminosity of component A. Following the expected $L^{1/4}$ dependence from Andrews et al. (2013), we might expect a factor of 2–3 increase in average dust temperature and a correspondingly decrease in the dust masses. These temperatures, masses, and mass ratios can only be estimates given the limited information but serve as a comparison with other millimeter wavelength disk observations.

The strong emission in multiple molecular lines suggests significant amounts of moderately warm and dense gas in both disks. The integrated line fluxes are only about a factor of 3–5 weaker in 253-1536B compared to the brighter millimeter component A, despite its much lower stellar luminosity. Radiation from the nearby primary member may be a significant factor in heating both disks and could potentially explain their roughly similar (to within $\sim$ 50%) line-to-continuum ratios. To compare the chemistry in the two disks, and also to measure their gas masses and gas-to-dust ratios, requires observations of optically thinner isotopologues (Williams & Best 2014).

Perhaps the most noteworthy result from these obser-

vations are that the projected disk rotational axes are highly misaligned, with an angle of $72\pm20^\circ$ to each other. As torques from the binary orbit act to align the disks on relatively short timescales (Lubow & Ogilvie 2000), the observed conditions are most likely a signature of their formation. Similar *ALMA* kinematic measurements of mis-alignment have been recently found in two other binary disk systems (Jensen & Akeson 2014; Salyk et al. 2014).

These observations demonstrate that wide binaries do not form from the same co-rotating structure such as a massive disk or coherent cloud core (Bodenheimer et al. 2000). Signatures of disorder from the early phases of star formation persist. One possibility is the fragmentation of a turbulent core (Offner et al. 2010; Tokuda et al. 2014). Numerical simulations shows that binary formation in even weakly turbulent cloud cores is quantitatively different than the purely thermal case (Tsukamoto & Machida 2013). In turbulent cores, the direction of angular momentum vectors vary with spatial scale such that disks may form at different angles from each other and from the overall core rotation axis (Bate 2012).

Alternatively, dynamical interactions of three or more protostars during the early Class O-I phases may chaotically scramble orbital axes. Non-hierarchical triple or small multiple systems with similar interstellar separations rapidly rearrange into hierarchical configurations consisting of a compact binary and distant companions or ejected members (Reipurth & Mikkola 2012; Reipurth et al. 2010). The observed decrease in multiplicity from Class 0 to I to main-sequence stars provides support for such dynamical evolution (Chen et al. 2013). In crowded regions, large disks may also assist in the capture of binaries, such as proposed for the massive star system Cepheus A (Cunningham et al. 2009). A similar event is thought to have occurred within the last 500 years in Orion BN/KL (Bally et al. 2011; Goddi et al. 2011).

Stellar rotation and orbital axes are more tightly aligned in closer systems, $a \lesssim 40\,\mathrm{AU}$ (Hale 1994), than those studied with *ALMA* to date. This is also seen in numerical simulations of cluster formation (Bate 2012). It would be interesting to search for disk alignment in such close binaries but, because the same proximity that might align the disks also tidally truncates them (Artymowicz & Lubow 1994; Andrews et al. 2010) and lowers their masses (Cieza et al. 2009), higher resolution and signal-to-noise observations than shown here will be required.

At larger scales, one can imagine larger studies across star forming complexes providing new information on the velocity dispersion of protostars in different evolutionary states that can constrain timescales and the turbulent properties of the cloud from which they formed. As disk surveys continue in new *ALMA* observing cycles, including an expanded program of Orion proplyds, we can expect to routinely detect a much broader suite of molecules and transitions than has been observed in all but a handful of the brightest disks to date. This will open up new paths of exploration for not only studying statistical disk properties such as masses, sizes, gas-to-dust ratios and chemistry, but also for examining the dynamics of young star forming regions.

We thank the referee for a very thorough report, Kaitlin Kratter, Stella Offner, and Hideko Nomura for comments, and Eric Jensen and Rachel Akeson for communicating their results ahead of publication. J.P.W. is supported by funding from the NSF through grant AST-1208911. D. J. is supported by the National Research Council of Canada and by a Natural Sciences and Engineering Research Council of Canada (NSERC) Discovery Grant. ALMA is a partnership of ESO (representing its member states), NSF (USA) and NINS (Japan), together with NRC (Canada) and NSC and ASIAA (Taiwan), in cooperation with the Republic of Chile. This work made use of Astropy, a community-developed core Python package for Astronomy (Astropy Collaboration et al. 2013).

Facilities: ALMA.

REFERENCES

Andrews, S. M., Czekala, I., Wilner, D. J., et al. 2010, ApJ, 710, 462
Andrews, S. M., Rosenfeld, K. A., Kraus, A. L., & Wilner, D. J. 2013, ApJ, 771, 129
Andrews, S. M., Wilner, D. J., Hughes, A. M., et al. 2012, ApJ, 744, 162
Artymowicz, P., & Lubow, S. H. 1994, ApJ, 421, 651
Astropy Collaboration, Robitaille, T. P., Tollerud, E. J., et al. 2013, A&A, 558, A33
Bally, J., Cunningham, N. J., Moeckel, N., et al. 2011, ApJ, 727, 113
Bate, M. R. 2012, MNRAS, 419, 3115
Batygin, K. 2012, Nature, 491, 418
Bodenheimer, P., Burkert, A., Klein, R. I., & Boss, A. P. 2000, Protostars and Planets IV, 675
Chen, X., Bourke, T. L., Launhardt, R., & Henning, T. 2008, ApJ, 686, L107
Chen, X., Arce, H. G., Zhang, Q., et al. 2013, ApJ, 768, 110
Cieza, L. A., Padgett, D. L., Allen, L. E., et al. 2009, ApJ, 696, L84
Cunningham, N. J., Moeckel, N., & Bally, J. 2009, ApJ, 692, 943
Desidera, S., & Barbieri, M. 2007, A&A, 462, 345
Duchêne, G., & Kraus, A. 2013, ARA&A, 51, 269
Goddi, C., Humphreys, E. M. L., Greenhill, L. J., Chandler, C. J., & Matthews, L. D. 2011, ApJ, 728, 15
Hale, A. 1994, AJ, 107, 306
Harris, R. J., Andrews, S. M., Wilner, D. J., & Kraus, A. L. 2012, ApJ, 751, 115
Hillenbrand, L. A. 1997, AJ, 113, 1733
Hughes, A. M., Wilner, D. J., Qi, C., & Hogerheijde, M. R. 2008, ApJ, 678, 1119
Jensen, E. L. N., & Akeson, R. 2014, Nature, 511, 567
Jensen, E. L. N., Mathieu, R. D., & Fuller, G. A. 1996, ApJ, 458, 312
Kraus, A. L., Ireland, M. J., Hillenbrand, L. A., & Martinache, F. 2012, ApJ, 745, 19
Lee, C.-F., Mundy, L. G., Stone, J. M., & Ostriker, E. C. 2002, ApJ, 576, 294
Lubow, S. H., & Ogilvie, G. I. 2000, ApJ, 538, 326
Mann, R. K., & Williams, J. P. 2009, ApJ, 699, L55
Mann, R. K., Di Francesco, J., Johnstone, D., et al. 2014, ApJ, 784, 82
Mathieu, R. D. 1994, ARA&A, 32, 465
Menten, K. M., Reid, M. J., Forbrich, J., & Brunthaler, A. 2007, A&A, 474, 515
O'dell, C. R., & Wen, Z. 1994, ApJ, 436, 194
Offner, S. S. R., Kratter, K. M., Matzner, C. D., Krumholz, M. R., & Klein, R. I. 2010, ApJ, 725, 1485
Ratzka, T., Schegerer, A. A., Leinert, C., et al. 2009, A&A, 502, 623
Reipurth, B., & Mikkola, S. 2012, Nature, 492, 221
Reipurth, B., Mikkola, S., Connelley, M., & Valtonen, M. 2010, ApJ, 725, L56
Ricci, L., Testi, L., Williams, J. P., Mann, R. K., & Birnstiel, T. 2011, ApJ, 739, L8
Roccatagliata, V., Ratzka, T., Henning, T., et al. 2011, A&A, 534, A33
Rosenfeld, K. A., Andrews, S. M., Wilner, D. J., & Stempels, H. C. 2012, ApJ, 759, 119
Salyk, C., Pontoppidan, K., Corder, S., et al. 2014, ApJ, 792, 68
Sandstrom, K. M., Peek, J. E. G., Bower, G. C., Bolatto, A. D., & Plambeck, R. L. 2007, ApJ, 667, 1161

Smith, N., Bally, J., Licht, D., & Walawender, J. 2005, AJ, 129, 382
Tobin, J. J., Hartmann, L., Chiang, H.-F., et al. 2012, Nature, 492, 83
Tokuda, K., Onishi, T., Saigo, K., et al. 2014, ApJ, 789, L4
Tsukamoto, Y., & Machida, M. N. 2013, MNRAS, 428, 1321
Williams, J. P., & Best, W. M. J. 2014, ApJ, 788, 59
Williams, J. P., & Cieza, L. A. 2011, ARA&A, 49, 67